COLD SPRING HARBOR
Molecular Case Studies

RESEARCH REPORT

A novel association of campomelic dysplasia and hydrocephalus with an unbalanced chromosomal translocation upstream of *SOX9*

Prince Antwi,[1] Christopher S. Hong,[1] Daniel Duran,[1] Sheng Chih Jin,[2] Weilai Dong,[2] Michael DiLuna,[1,3] and Kristopher T. Kahle[1,3,4]

[1]Department of Neurosurgery, Yale University School of Medicine, New Haven, Connecticut 06520, USA; [2]Department of Genetics, Yale University School of Medicine, New Haven, Connecticut 06520, USA; [3]Department of Pediatrics, Yale School of Medicine, New Haven, Connecticut 06520, USA; [4]Department of Cellular & Molecular Physiology, Yale School of Medicine, New Haven, Connecticut 06520, USA

Abstract Campomelic dysplasia is a rare skeletal dysplasia characterized by Pierre Robin sequence, craniofacial dysmorphism, shortening and angulation of long bones, tracheobronchomalacia, and occasionally sex reversal. The disease is due to mutations in *SOX9* or chromosomal rearrangements involving the long arm of Chromosome 17 harboring the *SOX9* locus. SOX9, a transcription factor, is indispensible in establishing and maintaining neural stem cells in the central nervous system. We present a patient with angulation of long bones and external female genitalia on prenatal ultrasound who was subsequently found to harbor the chromosomal abnormality 46, XY, t(6;17) (p21.1;q24.3) on prenatal genetic testing. Comparative genomic hybridization revealed deletions at 6p21.1 and 17q24.3, the latter being 2.3 Mb upstream of *SOX9*. Whole-exome sequencing did not identify pathogenic variants in *SOX9*, suggesting that the 17q24.3 deletion represents a translocation breakpoint farther upstream of *SOX9* than previously identified. At 2 mo of age the patient developed progressive communicating ventriculomegaly and thinning of the cortical mantle without clinical signs of increased intracranial pressure. This case suggests ventriculomegaly in some cases represents not a primary impairment of cerebrospinal fluid dynamics, but an epiphenomenon driven by a genetic dysregulation of neural progenitor cell fate.

[Supplemental material is available for this article.]

Corresponding author:
kristopher.kahle@yale.edu

Ontology terms: congenital kyphoscoliosis; hydrocephalus; sex reversal

Published by Cold Spring Harbor Laboratory Press

doi: 10.1101/mcs.a002766

INTRODUCTION

Named for the abnormal curvature of long bones seen in most patients, campomelic dysplasia (CMPD; Greek: *campto* = bent and *melia* = *limb*; OMIM #114290) is a rare skeletal dysplasia reported in 1:40,000 to 1:80,000 births (Unger et al. 2008 [updated: 2013]). Patients frequently present with bowing of the long bones, Pierre Robin sequence (PRS; i.e., cleft palate, glossoptosis, and micrognathia), tracheobronchomalacia, sex reversal in genotypic males, and 11 pairs of gracile ribs (Mansour et al. 2002; Unger et al. 2008 [updated: 2013]). Central nervous system (CNS) involvement may include kyphoscoliosis, hypoplastic olfactory tract, cerebral atrophy, and ventriculomegaly (Mansour et al. 2002; Matsumoto et al. 2017). A variant of CMPD, acampomelic campomelic dysplasia (ACMPD), is seen in ~10% of cases and

lacks involvement of long bones (Walters-Sen et al. 2014). CMPD is lethal in the neonatal period, but patients with less severe phenotypes may survive (Maroteaux et al. 1971).

Mutations and chromosomal arrangements that affect expression and/or activity of *SOX9* are implicated in CMPD (Unger et al. 2008 [updated: 2013]). Several cases of CMPD/ACMPD due to translocations upstream of *SOX9* have been reported (Walters-Sen et al. 2014). Here, we report a 3-mo-old patient found to have skeletal anomalies on prenatal ultrasound and unbalanced translocation t(6;17) (p21.1;q24.3) with deletions on prenatal genetic testing. Located 2.3 Mb upstream of *SOX9*, the translocation configures a previously unreported breakpoint cluster on Chromosome 17. Postnatal radiographs, clinical features, and genetic testing were consistent with CMPD. This patient came to the attention of our pediatric neurosurgical service because of acquired diffuse ventriculomegaly at 2 mo of age. Additionally, respiratory compromise, likely due to tracheobronchomalacia, was noted at this time. This case demonstrates the clinical, radiographic, and genetic features of CMPD, introduces a novel breakpoint, and suggests a new cluster of noncoding region that likely controls *SOX9* expression.

RESULTS

Clinical Presentation and Treatment

The patient was born at 39 wk of gestation to a G_3P_{2012} mother in a nonconsanguineous marriage who had a previous chemical pregnancy. Ultrasound obtained at 20 wk of gestation showed bowed femurs and right tibia, increased nuchal thickness (6.2 mm), and female external genitalia. No intracranial abnormalities were identified. Amniocentesis was performed at 21 wk of gestation, revealing a normal level of α-fetoprotein (5748 ng/ml; Yale New Haven Hospital Laboratory). Cytogenetic analysis on cultured amniocytes was then pursued. The parents were counseled on the likelihood of the fetus having CMPD given radiographic and genetic findings (discussed in detail under Genetic Analysis); a decision was reached to continue gestation to term.

The patient was delivered by elective cesarean section because of breech presentation. She demonstrated respiratory distress at birth, requiring immediate intubation and admission to the neonatal intensive care unit. She additionally demonstrated a Veau 2 cleft palate, mild retrognathia, and hypertelorism. Shortly after delivery, magnetic resonance imaging (MRI) of the head (protocoled to study the skull base, sinonasal, and facial regions) demonstrated craniofacial defects including cleft hard palate, leftward deviation of nasal septum, hypoplastic mandible and maxilla, and 45° vertical angulation of the skull base. No intracranial abnormalities were noted (Fig. 1A,C,E). MRI of the spine was notable for hypoplastic C6 vertebral body, exaggerated cervical lordosis, and exaggerated thoracic kyphosis resulting in severe canal stenosis at T1–4 (Fig. 2). A pelvic ultrasound showed a normal appearing uterus and a hypoplastic right ovary; the left ovary was not visualized. A subsequent skeletal X-ray survey revealed angulated left femoral shaft, hypoplastic pubic bones, and absent ossification of the right talus (Fig. 3). After 31 d in the intensive care unit, the patient was discharged with plans for multidisciplinary outpatient management including neurosurgical follow-up.

At 2 mo of age the patient was readmitted for lethargy and acute respiratory distress. Chest X-ray showed focal basilar consolidations. A head ultrasound was notable for ventriculomegaly, for which neurosurgery was consulted. On neurological examination, the patient spontaneously opened eyes with briskly reactive pupils, moved all extremities to light stimulation, exhibited flat and soft fontanels, and had a head circumference of 40 cm (90th percentile). There were no clinical signs of increased intracranial pressure (ICP). Subsequent MRI brain (protocoled with a T2 cine flow study) revealed globally dilated ventricles with marked

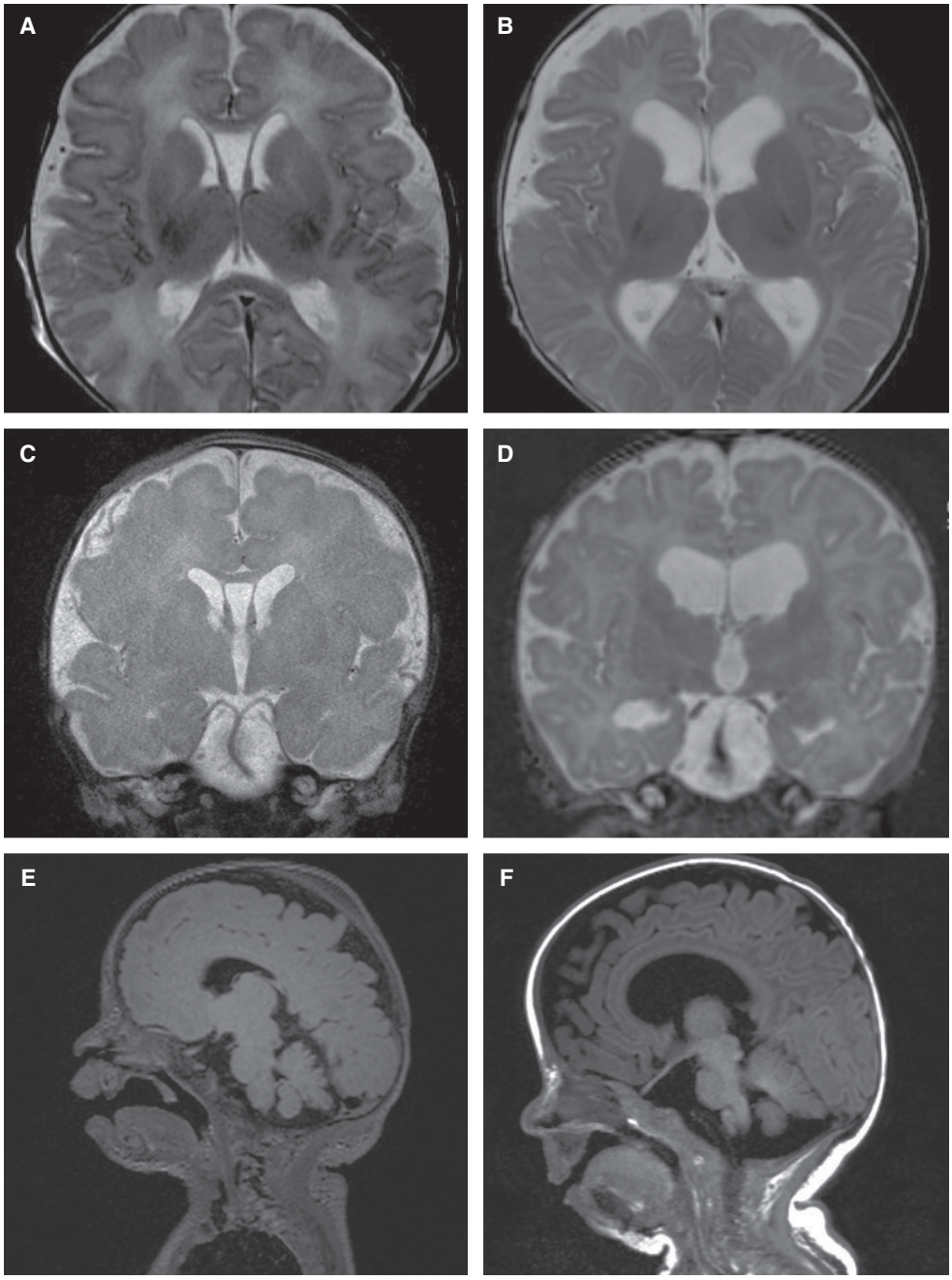

Figure 1. Acquired diffuse ventriculomegaly as a manifestation of campomelic dysplasia. At birth the patient had no radiographic evidence of ventriculomegaly (see axial T2-weighted, reformatted coronal, and sagittal FLAIR images in *A*,*C*,*E*). At 2 mo old she had lateral, third, and fourth ventriculomegaly but no clinical evidence of increased intracranial pressure (ICP) (*B*,*D*,*F*).

prominence of the basal, prepontine, and suprasellar cisterns, enlarged bifrontal extra-axial spaces, development of a mega cisterna magna, and patent flow around the foramen magnum (Fig. 1B,D,F). Computerized tomography (CT) evaluation of the spine revealed gracile ribs, narrowed spinal canal at the cervicothoracic junction, and narrowed thoracic cage. The

Figure 2. Spinal involvement in campomelic dysplasia. Our patient demonstrated exaggerated cervical lordosis and thoracic kyphosis. Notice moderate-to-severe stenosis of the spinal canal from T1/2 to T3/4 on the sagittal isotropic T2-weighted image. Image artifact from bed support is present.

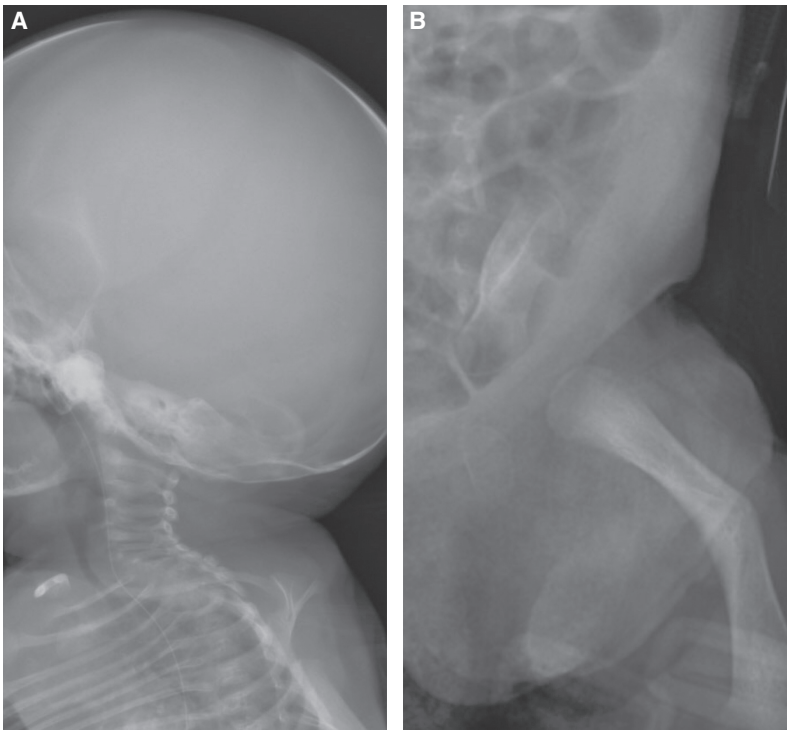

Figure 3. Skeletal features of campomelic dysplasia. Skeletal involvement in CMPD may include (*A*) pairs of gracile ribs, exaggerated lordosis of the cervical spine (often associated with hypoplastic cervical vertebral bodies), and (*B*) shortening and angulation of long bones (usually of the lower extremities).

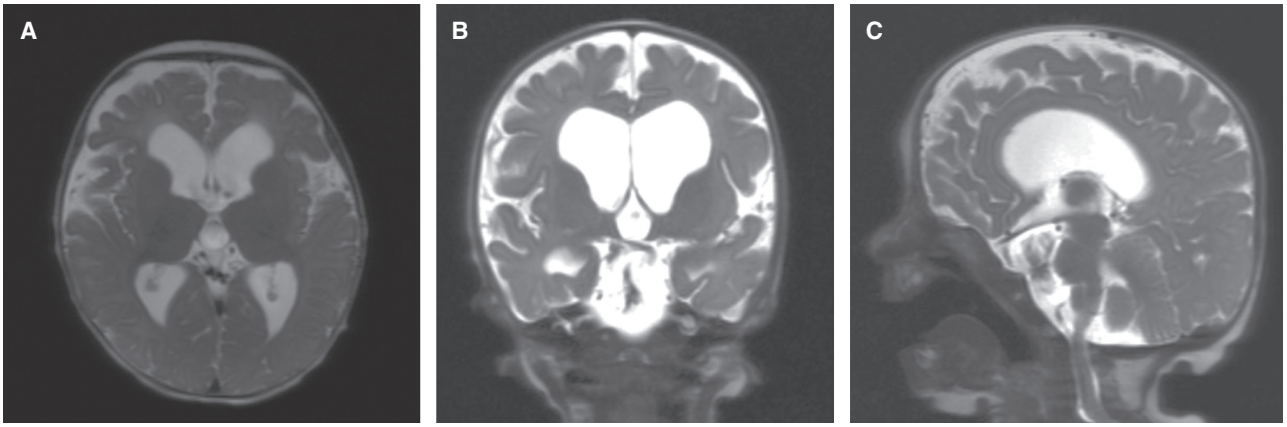

Figure 4. Worsening acquired ventriculomegaly in CMPD. At 3 mo of age, surveillance (*A*) axial, (*B*) coronal, and (*C*) sagittal T2-weighted MRI demonstrate worsening ventriculomegaly, although the patient showed no clinical signs of increased intracranial pressure (ICP).

patient's neurologic exam was monitored over several days for signs of increased ICP with plans for a possible external ventricular drain, but she showed no such signs. She required mechanical ventilation and later tracheostomy for ventilator support. Surveillance MRI obtained at 3 mo of age revealed worsening ventriculomegaly in spite of the patient showing no clinical signs of increased ICP (Fig. 4).

Genetic Analysis

All procedures reported comply with Yale University's Human Investigation Committee and Human Research Protection Program. Written consent from both parents was obtained prior to genetic testing. All reported genomic coordinates reference the human genome assembly (GRCh37/hg19).

Fluorescence in situ hybridization (FISH; using probes for RB1 at 13q14, D21S259, Xcen, Ycen, and D18Z1; Vysis Inc.) of cultured amniocytes obtained at 21 wk of gestation demonstrated normal Chromosomes 13, 18, 21, X, and Y and the presence of the SRY locus. It additionally revealed an apparently balanced translocation between chromosomal bands 6p21.1 and 17q24: 46, XY, t(6;17) (p21.1;q24.3) (Fig. 5). Concurrent array comparative genomic hybridization (aCGH; Agilent 180K) analysis on DNA extracted from cultured amniocytes was performed. It showed an XY male with a 125 kb deletion at 6p21.1 (Chr 6:41,621,953–41,746,502) and a 97 kb deletion at 17q24.3 (Chr 17:67,666,390-67,762,983). The deletion at 6p21.1 includes *MDFI*, *TFEB*, *PGC*, and *FRS3*; the deletion at 17q24.3 contains no genes and is ~2.3 Mb upstream of *SOX9* (Chr 17:70,117,161–70,122,561). Contrasting results between FISH and array comparative genomic hybridization (aCGH) ascertained an unbalanced translocation. Karyotype and aCGH (using Agilent 400K) of cultured stimulated peripheral lymphocytes from proband's mother revealed a normal female complement. Karyotype and aCGH (using Agilent 180K) of cultured stimulated peripheral lymphocytes from proband's father revealed a normal male complement.

The absence of chromosomal rearrangements on genetic testing of parents suggested that the unbalanced translocation in the proband most likely occurred de novo. Postnatal FISH (Cytocell Inc.) and cytogenetics using peripheral blood samples from the proband corroborated results of the prenatal genetic studies.

When the patient was readmitted at 2 mo of age, a peripheral blood sample was obtained for high-throughput whole-exome sequencing (WES; using Roche/Nimblegen

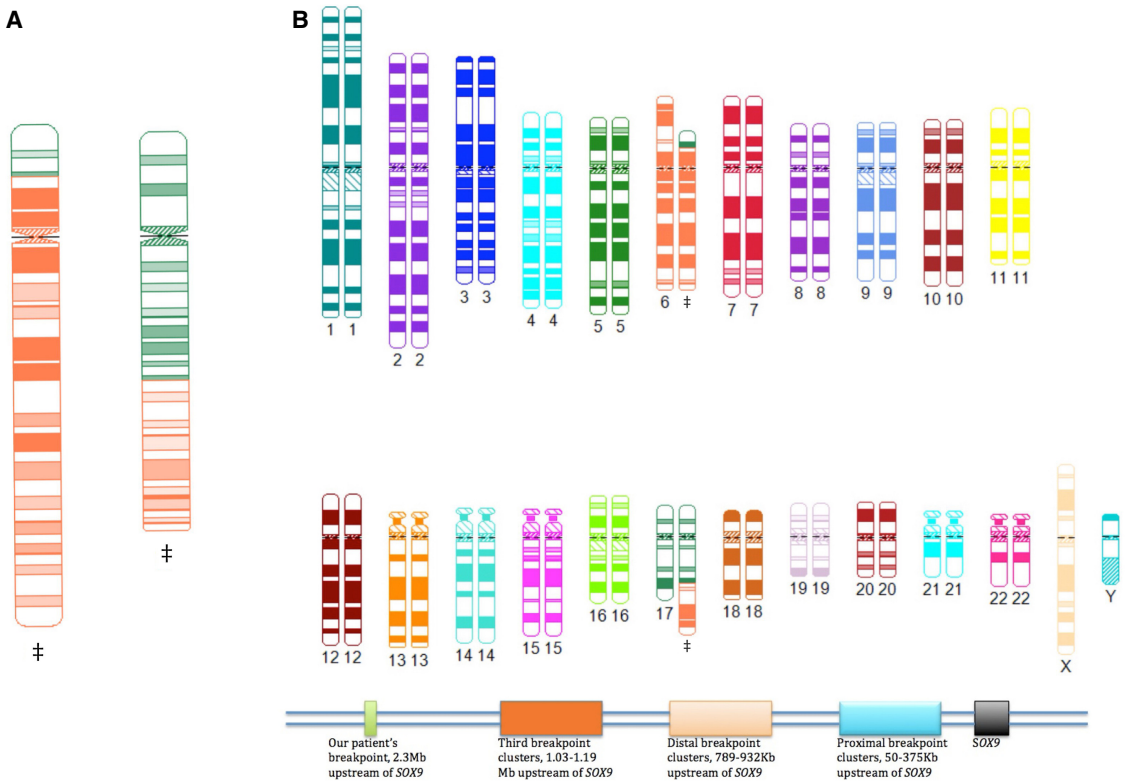

Figure 5. Ideogram and karyogram of patient. (*A*) Ideogram and (*B*) karyogram demonstrating the unbalanced translocation in our patient. At the *bottom* of *B* is a schema demonstrating the approximated relation of our patient's breakpoint site on Chromosome 17 to previously reported breakpoint sites in CMPD. ‡ denotes chromosomes with translocated segments in our patient. (Used: Hiller B, Bradtke J, Balz H, Rieder H [2004]: "CyDAS Online Analysis Site"; http://www.cydas.org/OnlineAnalysis/.)

MedExome and Illumina HiSeq platform). It showed that 98.8% of targeted bases had eight or more independent reads, and 98.6% had 15 or more (see Supplemental Table 4 for WES coverage metrics). No pathogenic variants were identified in *SOX9*, and the deletion at 17q24.3 was not present, suggesting that CMPD in our patient was likely due to the unbalanced translocation at a noncoding locus on Chromosome 17 (see Table 1 for genetic variants).

DISCUSSION

We present a patient with CMPD with skeletal, CNS, pulmonary, and genitourinary involvement due to an unbalanced t(6;17) (p21.1;q24.3). Bowing of the long bones of the lower extremities and increased nuchal thickness on second trimester ultrasound study raised suspicion for a chromosomal abnormality in this patient. Prenatal genetic testing revealed 46, XY, t(6;17) (p21.1;q24.3) with a 125-kb deletion on Chromosome 6 and a 97-kb deletion on Chromosome 17, demonstrating a novel breakpoint 2.3 Mb upstream of *SOX9* (Wirth et al. 1996; Walters-Sen et al. 2014). Postnatal WES revealed no pathogenic variants of *SOX9*, suggesting that the unbalanced translocation may be related to CMPD with sex reversal in our patient. At 2 mo of age, she had developed progressive communicating ventriculomegaly with normal ICP.

Table 1. Germline variants identified in the patient

Gene	Chr-pos-ref-alt	HGVS alterations	Variant type	Predicted effect (PolyPhen)	MetaSVM	CADD	dbSNP	ExAC	pLI	mis_Z
Heterozygous variants										
LAMB2	3-55369293-GA-G	p.Ser1169fs	fs_deletion	N/A	N/A	N/A	N/A	N/A	0.00	1.61
TRIM4	7-53226946-GCTGA-G	p.Ser194fs	fs_deletion	N/A	N/A	N/A	N/A	N/A	0.00	0.29
BECN1	17-40963699-GC-G	p.Gly386fs	fs_deletion	N/A	N/A	N/A	N/A	N/A	1.00	1.57
SPAG17	1-114304570-T-TATTTG	p.Tyr1296fs	fs_insertion	N/A	N/A	N/A	N/A	N/A	0.00	−2.39
DIMT1	5-14031721-T-TAA	p.Val207fs	fs_insertion	N/A	N/A	N/A	N/A	N/A	0.00	0.36
SLC27A6	5-19369362-G-A	c.1454+1G>A	Splicing	N/A	N/A	26.1	rs779289426	4.14×10^{-5}	0.00	−1.24
PAPPA2	1-19207800-C-T	p.Gln443*	Stop-gain	N/A	N/A	33.0	N/A	N/A	0.00	0.13
ADRA2B	2-119993667-C-T	p.Trp112*	Stop-gain	N/A	N/A	36.0	N/A	N/A	0.00	0.52
MRPL44	2-33349186-C-T	p.Gln106*	Stop-gain	N/A	N/A	36.0	rs769072268	3.30×10^{-5}	0.00	−0.11
UGT2A3	4-20109056-A-T	p.Leu121*	Stop-gain	N/A	N/A	28.1	N/A	N/A	0.00	−3.21
FGF5	4-40963699-T-A	p.Leu3*	Stop-gain	N/A	N/A	36.0	N/A	N/A	0.00	−0.58
H6PD	1-179143220-C-T	p.Ala153Val	Missense	D	D	31.0	N/A	N/A	0.00	−0.73
GBA	1-69970145-G-A	p.Pro358Leu	Missense	D	D	27.6	N/A	N/A	0.03	2.06
CANX	5-39307740-C-T	p.Pro279Leu	Missense	D	D	32.0	rs769363661	4.12×10^{-5}	0.86	0.92
GAS1	9-60498743-G-C	p.Arg45Gly	Missense	D	D	25.9	N/A	N/A	0.62	4.27
CSRP3	11-19207800-G-A	p.Ser126Leu	Missense	B	D	23.7	N/A	N/A	0.00	−0.66
GCH1	14-55369293-G-C	p.Pro30Arg	Missense	B	D	16.3	N/A	N/A	0.94	2.91
SMPD3	16-68404920-C-T	p.Val389Ile	Missense	P	D	22.6	rs757669112	4.97×10^{-5}	0.66	0.34
DNM2	19-10939884-T-C	p.Val744Ala	Missense	B	D	11.8	rs777609224	2.49×10^{-5}	1.00	4.61
DOK5	20-53226946-G-A	p.Gly99Arg	Missense	D	D	34.0	N/A	N/A	0.04	1.18
PITHD1	1-38702298-C-G	p.Thr164Arg	Missense	B	T	23.0	rs763501501	3.31×10^{-5}	0.10	1.58
DNAJB4	1-99506417-C-T	p.Arg47Trp	Missense	P	T	24.8	rs756468720	1.67×10^{-5}	0.84	0.13
HENMT1	1-89561562-A-C	p.Leu347Arg	Missense	P	T	22.5	rs755233826	8.24×10^{-6}	0.00	−0.42
METTL18	1-4661109-A-G	p.Val334Ala	Missense	B	T	22.7	N/A	N/A	0.03	−1.40
PTPN14	1-61040701-C-T	p.Arg8His	Missense	P	T	34.0	N/A	N/A	0.99	1.53
FMNL2	2-27087562-G-T	p.Ser160Ile	Missense	B	T	20.4	rs866373641	N/A	1.00	1.50
IQCA1	2-23518359-C-T	p.Arg220His	Missense	B	T	25.6	rs563978762	1.33×10^{-5}	0.00	−0.99
STX19	3-57700600-T-C	p.Tyr151Cys	Missense	D	T	24.7	rs759950914	8.24×10^{-6}	0.00	−1.93
RPN1	3-846041-G-A	p.Ala566Val	Missense	B	T	23.0	rs754321104	3.30×10^{-5}	0.66	0.87
PLXND1	3-68404920-G-A	p.Ala562Val	Missense	P	T	22.7	rs746020904	2.43×10^{-5}	1.00	4.48
YEATS2	3-8167903-C-T	p.His1228Tyr	Missense	B	T	25.2	rs749637060	1.66×10^{-5}	1.00	−0.81
FAT4	4-72725470-C-T	p.Pro4564Leu	Missense	P	T	27.9	N/A	N/A	1.00	−0.32
C7	5-10939884-C-A	p.Asp453Glu	Missense	P	T	25.2	N/A	N/A	0.00	−2.57
MAP1B	5-15276648-G-A	p.Asp1758Asn	Missense	B	T	24.1	N/A	N/A	1.00	2.04
DNAH8	6-52793840-A-T	p.Lys220Ile	Missense	P	T	23.2	N/A	N/A	0.00	−0.94
ZNF483	9-61919093-C-T	p.Ala452Val	Missense	B	T	24.4	rs751071638	1.66×10^{-5}	0.41	1.89
MYPN	10-35808610-C-T	p.Ser1005Phe	Missense	B	T	25.6	rs748628394	8.24×10^{-6}	0.07	−0.35
OR51D1	11-4661109-C-T	p.Pro30Leu	Missense	D	T	24.6	N/A	N/A	0.00	−2.06
VWCE	11-61040701-A-G	p.Phe557Leu	Missense	B	T	23.7	rs752514073	N/A	0.00	0.38
TRIM29	11-119993667-G-C	p.Pro477Arg	Missense	P	T	23.7	N/A	N/A	0.00	0.38

(*Continued on next page.*)

Table 1. (*Continued*)

Gene	Chr-pos-ref-alt	HGVS alterations	Variant type	Predicted effect (PolyPhen)	MetaSVM	CADD	dbSNP	ExAC	pLI	mis_Z
INTS13	12-27087562-A-G	p.Val76Ala	Missense	B	T	26.3	N/A	N/A	N/A	N/A
PDS5B	13-33349186-G-A	p.Arg1447Gln	Missense	D	T	24.1	N/A	N/A	1.00	3.56
CDH24	14-23518359-T-G	p.Ser613Arg	Missense	D	T	22.7	N/A	N/A	0.00	2.75
EXOC5	14-57700600-C-T	p.Gly239Asp	Missense	B	T	21.9	rs753219587	2.49×10^{-5}	1.00	1.36
CHTF18	16-846041-G-A	p.Arg807His	Missense	B	T	23.1	rs756795078	2.61×10^{-5}	N/A	N/A
PFAS	17-8167903-G-A	p.Arg678His	Missense	D	T	34.0	rs772566332	4.99×10^{-5}	0.00	0.80
SPECC1	17-20109056-C-A	p.Ala565Asp	Missense	P	T	22.8	N/A	N/A	0.11	−1.11
RAB37	17-72725470-G-A	p.Gly50Ser	Missense	P	T	23.9	rs753157903	1.65×10^{-5}	0.00	0.12
CC2D1A	19-14031721-G-A	p.Val543Met	Missense	D	T	25.2	N/A	N/A	0.00	0.52
NOTCH3	19-15276648-G-A	p.Arg1873Cys	Missense	D	T	33.0	rs749429793	8.37×10^{-6}	0.21	4.79
HAPLN4	19-19369362-C-G	p.Asp263His	Missense	D	T	28.3	N/A	N/A	0.03	2.94
ECH1	19-39307740-G-A	p.Arg185Trp	Missense	D	T	33.0	N/A	N/A	0.00	0.00
ZNF766	19-52793840-A-C	p.Thr266Pro	Missense	D	T	23.1	rs772342873	2.51×10^{-5}	0.00	−1.10
CDH4	20-60498743-T-C	p.Phe537Leu	Missense	B	T	21.6	rs767012233	8.30×10^{-6}	0.97	2.39
ARFGAP1	20-61919093-C-G	p.Ser371Arg	Missense	D	T	28.4	rs756425439	4.07×10^{-5}	0.02	−0.30
MCM5	22-35808610-A-C	p.Ile343Leu	Missense	B	T	24.5	rs773193463	8.43×10^{-6}	0.56	1.74
Homozygous variants										
SLAIN1	13-78272267-T-TGG	p.Ala73fs	fs_insertion	N/A	N/A	N/A	rs201380414	0	0.96	1.19
X-linked hemizygous variants										
RS1	X-18665373-C-G	p.Gln88His	Missense	D	D	19.9	rs201680258	3.00×10^{-4}	0.89	1.51
SHROOM2	X-9914844-C-T	p.Ala1573Val	Missense	P	T	24.6	rs767591095	4.10×10^{-5}	0.01	−1.23

HGVS, Human Genome Variation Society; CADD, Combined Annotation Dependent Depletion; N/A, not available; fs, frameshift; PolyPhen: "B"enign, "D"amaging, "P"otentially/probably damaging; MetaSVM: "D"eleterious, "T"olerated.

SOX9, located at 17q24.3, is the only gene with known pathogenic variants that cause CMPD (Fonseca et al. 2013; Symon and Harley 2017). SOX9 belongs to the Sry-related high-mobility group (HMG) of transcriptional regulators and is involved in chrondrogenesis, craniofacial development, male sex determination, and neural stem cell development (Cheung and Briscoe 2003; Finzsch et al. 2008; Scott et al. 2010; Lee and Saint-Jeannet 2011; Symon and Harley 2017).

We identified a de novo unbalanced translocation associated with this case of CMPD. De novo translocations involving 17q24.3–25.1 represent <5% of cases of CMPD (Unger et al. 2008 [updated: 2013]). Reported translocations upstream of *SOX9* include t(1;17), t(2;17), t(4;17), t(5;17), t(6;17), t(7;17), t(9;17), t(10;17), t(12;17), t(13;17), t(17;20), and t(17;22) (Young et al. 1992; Tommerup et al. 1993; Foster et al. 1994; Wagner et al. 1994; Ninomiya et al. 1996; Wirth et al. 1996; Savarirayan and Bankier 1998; Wunderle et al. 1998; Pfeifer et al. 1999; Hill-Harfe et al. 2005; Velagaleti et al. 2005; Leipoldt et al. 2007; Fonseca et al. 2013; Matsumoto et al. 2017). Our patient had t(6;17) which has been reported in two previous cases. Wirth et al. (1996) reported a patient who demonstrated PRS, dysplastic iliac wings and femur, closed cranial sutures, and external female genitalia. Cytogenetics revealed 46, XY, t(6;17) (q14;q24) in this patient. Walters-Sen et al. (2014) reported an infant who presented with PRS, cervical spine deformities, hypoplastic scapulae, external female genitalia, and no involvement of the long bones. Genetic analysis revealed a 46, XY,

t(6;17) (q25;q24) in this case of ACMPD. Our patient had the breakpoint at (p21.1;q24.3) with a 125-kb deletion at 6p21.1 (including *MDF1*, *TFEB*, *PGC*, and *FRS3*) and a 97-kb deletion at 17q24.3, which contains no genes. In silico analyses of WES data identified a 74-kb deletion at 6p21.1 (6:41,691,198–41,765,585) that includes *TFEB*, *PGC*, *FRS3*, *PRICKLE4*, *TOMM6*. There are no known phenotypic correlates of *MDF1*, *PGC*, *TOMM6*, *PRICKLE4*, and *FRS3* in the OMIM database; the *TFEB* deletion has been reported in renal cell carcinoma (OMIM # 600744). The 17q24.3 deletion contained no genes, is located upstream of *SOX9*, does not overlap with previous deletions reported in CMPD, and likely affects expression of SOX9 (Velagaleti et al. 2005; Gordon et al. 2009; Walters-Sen et al. 2014). The deleted region of Chromosome 17 is a binding site for multiple transcription factors, including SETDB1 and KAP1 that interact with SOX9 in chondrogenesis and sex determination, respectively (Peng et al. 2009; Yahiro et al. 2017). In silico analyses revealed no other rare genetic variant associated with CMPD (see Supplemental Table 1).

It has been suggested that proximity of breakpoints to the *SOX9* locus is correlated with the severity of CMPD (Leipoldt et al. 2007; Walters-Sen et al. 2014). Interestingly, the breakpoint in our case is 2.3 Mb upstream of *SOX9*, more distal than previously described clusters of Chromosome 17 breakpoint sites in the disease, yet our patient had a severe phenotype of CMPD. Leipoldt et al. (2007) described proximal (50–375 kb) and distal (789–932 kb) clusters of translocation breakpoints in CMPD. More recently, cases with breakpoint clusters farther upstream of *SOX9* (1.03–1.19 Mb) have been reported, creating a third cluster that is often seen in patients with isolated PRS (Jamshidi et al. 2004; Jakobsen et al. 2007; Benko et al. 2009; Walters-Sen et al. 2014). Our case demonstrates a cluster of breakpoints more than 2 Mb upstream of *SOX9* that is associated with severe disease phenotype.

When our patient was readmitted at 2 mo of age for lethargy and respiratory distress, head ultrasound and a brain MRI revealed diffuse ventriculomegaly (Fig. 1). Radiographic evaluation of the brain shortly after birth did not reveal ventriculomegaly, and we cannot ascertain when the patient developed this less common manifestation of CMPD. In the absence of signs of increased ICP, no immediate neurosurgical interventions were necessary. Matsumoto et al. (2017) recently reported a case of acquired ventriculomegaly and thinning of the corpus callosum in an 18 mo old born with normal cranial imaging and ACMPD due to a de novo missense mutation in *SOX9*. Ventriculomegaly observed in their patient was likely due to an ex vacuo phenomenon with expected absence of elevated ICP. Our patient showed thinning of the cortical mantle on MRI, but we acknowledge that, without tissue analysis, abnormal neuronal development cannot be established. Regardless, our patient exhibited similar features of normal ICP and communicating hydrocephalus with no indication for CSF diversion, raising the possibility that the ventriculomegaly observed in CMPD may be compensatory and does not necessitate neurosurgical intervention. Further clinical reports are needed to corroborate this hypothesis.

In murine models, mutation of *Sox9* resulted in diminished number of oligodendrocytes in early spinal cord development only to be rescued by *Sox8* expression later in development (Cheung and Briscoe 2003; Finzsch et al. 2008). Potentially, a similar mechanism in the cerebrum accounts for ventriculomegaly, thinning of the corpus callosum, hypoplastic olfactory tract, and cerebral atrophy observed in some patients with CMPD. In experiments investigating CNS development in mice and chicks, Scott et al. (2010) observed that induction of SOX9 in neural cells coincides with the presence of neural stem cells that generate neurons and glial cells. Further, loss of *Sox9* expression resulted in ependymal cells adopting a neuroblast identity. Impaired differentiation and ciliation of ependymal cells may account for the ventriculomegaly observed in CMPD, as has been reported in deletion of *SXN27*, a gene that encodes an endosomal sorting factor responsible for trafficking transmembrane receptors in the brain (Wang et al. 2016). Future studies may investigate this hypothesis.

Although the diagnosis of CMPD/ACMPD is typically made on clinical and radiographic grounds, genetic testing for mutations in *SOX9* or chromosomal rearrangements involving Chromosome 17 should be pursued. Genetic testing identifies pathogenic variants of *SOX9* or chromosomal rearrangements in 95% of cases (Unger et al. 2008 [updated: 2013]). CMPD is inherited in an autosomal dominant fashion, but most cases are due to de novo genetic alterations. Parental mosaicisim should be considered too. Genetic counseling should be availed to families of patients with this disease. Management of CMPD requires multidisciplinary care. Mortality rate remains high at 77% and 90% by 1 mo old and 2 yr old, respectively; a few patients with less severe phenotypes survive to reproductive age (Maroteaux et al. 1971; Mansour et al. 2002).

METHODS

Sample Collection and Processing

Following informed consent, cultured amniocytes of the proband were obtained at 21 wk of gestation for prenatal FISH and aCGH; cultured peripheral lymphocytes of the proband's parents were also obtained for karyotypes and aCGH studies. Postnatally, the proband's peripheral blood sample was obtained for WES.

Cytogenetics

Proband

FISH was performed on culture amniocytes using tricolor probes (Vysis Inc.) for DXZ1 locus at Xcen, DYZ3 locus at Ycen, and D18Z1 locus at 18cen, dual-color probes (Vysis Inc.) for 13q14 and D21S259 locus at 21q22, and tricolor probes (Cytocell Inc.) for the *SRY* gene at Yp11.2, DYZ1 locus at Yq12, and DXZ1 locus at Xcen. Chromosome microarray analysis was performed on an array of 180,000 oligonucleotide probes covering the whole genome (Agilent 180K), using high-molecular-weight DNA extracted from the culture amniocytes.

Proband's Parents

Cultured stimulated peripheral lymphocytes in metaphase were stained using standard technique. In the proband's mother, a chromosome microarray analysis was performed on an array of 400,000 oligonucleotide copy number and single-nucleotide polymorphism (SNP) probes covering the whole-genome (Agilent 400K CGH/SNP), using high-molecular-weight DNA extracted from the mother's blood specimen. aCGH in proband's father was performed similarly (using Agilent 180K and peripheral blood specimen) as described for the proband above.

Exome Sequencing

Genomic DNA was extracted and purified from the proband's peripheral blood using standard protocol at the Yale Center for Genome Analysis. Human genes were isolated by array capture (Roche/Nimlegen MedExome), and these genes were sequenced on the Illumina HiSeq platform as previously described (Duran et al. 2016; Jin et al. 2017). Sequence reads were independently mapped to the reference genome (GRCh37/hg19) with BWA-MEM and further processed using GATK Best Practices workflows (McKenna et al. 2010; Van der Auwera et al. 2013; Genomes Project Consortium et al. 2015), including duplication marking, indel realignment, and base quality recalibration, as previously described (Jin et al. 2017). Using these techniques, mean coverage of the exome is 60×–100×; 96%–97% of the exome is covered at least eight times, and 90%–95% is covered at >20×. The exome sequencing

metrics in our patient are provided in Supplemental Table 4. Single-nucleotide variants and small indels were called with GATK HaplotypeCaller and annotated using ANNOVAR (Wang et al. 2010), dbSNP (v138), 1000 Genomes (August 2015), NHLBI Exome Variant Server (EVS), and ExAC (v3) (Lek et al. 2016). The MetaSVM (Dong et al. 2015) and the Combined Annotation Dependent Deletion (CADD; v1.3) (Kircher et al. 2014) algorithms were used to predict the deleteriousness of missense variants.

Variant Filtering

Variants were filtered for relevance to human disease based on population frequency, likelihood of affecting protein function, and available information in disease-specific databases. The following criteria were used for determining dominant variants in our patient: Remove GATK Variant Score Quality Recalibration (VSQR) <"PASS"; remove known false positives; remove coverage <eight reads in proband, remove Genotype Quality (GQ) <20; remove global minor allele frequency (MAF) $>5 \times 10^{-5}$ in ExAC, 1000 Genomes, and EVS. Loss of function (i.e., frameshift, canonical splice site, stop-gain, and stop-loss) and MetaSVM "D"eleterious missense and CADD ≥20 missense variants were kept. For homozygous/X-linked hemizygous variants, those that met the following criteria were removed: GATK VSQR <"PASS", known false positives, coverage <eight reads in proband, GQ <20, global MAF $>1 \times 10^{-3}$ in ExAC, 1000 Genomes, and EVS. Loss of function, MetaSVM "D"eleterious missense, and CADD ≥20 missense variants were kept.

ADDITIONAL INFORMATION

Data Deposition and Access

The t(6;17) translocation in this paper has been submitted to ClinVar (https://www.ncbi.nlm.nih.gov/clinvar/) under accession number SCV000734849. Raw sequencing data were not deposited in the absence of patient consent but may be available by contacting the authors.

Ethics Statement

All procedures reported comply with Yale University's Human Investigation Committee and Human Research Protection Program. Written consent from both parents was obtained prior to genetic testing.

Acknowledgments

We sincerely appreciate the parents of our patient for agreeing to have us present this case to the medical community. We also thank our colleagues who helped manage the patient presented in this report.

Competing Interest Statement

The authors have declared no competing interest.

Referees

Peter J. Hurlin
Akash Kumar
Anonymous

Received February 6, 2018; accepted in revised form March 26, 2018.

Author Contributions

All authors were involved in the conception and design of the study, analysis and interpretation of data, drafting the article, and critically revising the article.

Funding

P.A. is supported by the National Institutes of Health (NIH) Clinical and Translational Science Award (CTSA) under Award Number TL1TR000141. S.C.J. is supported by the James Hudson Brown-Alexander Brown Coxe Postdoctoral Fellowship at the Yale University School of Medicine. K.T.K. is supported by the Hydrocephalus Foundation, March of Dimes, and NIH.

REFERENCES

Benko S, Fantes JA, Amiel J, Kleinjan DJ, Thomas S, Ramsay J, Jamshidi N, Essafi A, Heaney S, Gordon CT, et al. 2009. Highly conserved non-coding elements on either side of SOX9 associated with Pierre Robin sequence. *Nat Genet* **41:** 359–364.

Cheung M, Briscoe J. 2003. Neural crest development is regulated by the transcription factor Sox9. *Development* **130:** 5681–5693.

Dong C, Wei P, Jian X, Gibbs R, Boerwinkle E, Wang K, Liu X. 2015. Comparison and integration of deleteriousness prediction methods for nonsynonymous SNVs in whole exome sequencing studies. *Hum Mol Genet* **24:** 2125–2137.

Duran D, Jin SC, DeSpenza T Jr, Nelson-Williams C, Cogal AG, Abrash EW, Harris PC, Lieske JC, Shimshak SJ, Mane S, et al. 2016. Digenic mutations of human OCRL paralogs in Dent's disease type 2 associated with Chiari I malformation. *Hum Genome Var* **3:** 16042.

Finzsch M, Stolt CC, Lommes P, Wegner M. 2008. Sox9 and Sox10 influence survival and migration of oligodendrocyte precursors in the spinal cord by regulating PDGF receptor α expression. *Development* **135:** 637–646.

Fonseca AC, Bonaldi A, Bertola DR, Kim CA, Otto PA, Vianna-Morgante AM. 2013. The clinical impact of chromosomal rearrangements with breakpoints upstream of the *SOX9* gene: two novel de novo balanced translocations associated with acampomelic campomelic dysplasia. *BMC Med Genet* **14:** 50.

Foster JW, Dominguez-Steglich MA, Guioli S, Kwok C, Weller PA, Stevanovic M, Weissenbach J, Mansour S, Young ID, Goodfellow PN, et al. 1994. Campomelic dysplasia and autosomal sex reversal caused by mutations in an SRY-related gene. *Nature* **372:** 525–530.

Genomes Project Consortium, Auton A, Brooks LD, Durbin RM, Garrison EP, Kang HM, Korbel JO, Marchini JL, McCarthy S, McVean GA, et al. 2015. A global reference for human genetic variation. *Nature* **526:** 68–74.

Gordon CT, Tan TY, Benko S, Fitzpatrick D, Lyonnet S, Farlie PG. 2009. Long-range regulation at the SOX9 locus in development and disease. *J Med Genet* **46:** 649–656.

Hill-Harfe KL, Kaplan L, Stalker HJ, Zori RT, Pop R, Scherer G, Wallace MR. 2005. Fine mapping of Chromosome 17 translocation breakpoints ≥900 Kb upstream of SOX9 in acampomelic campomelic dysplasia and a mild, familiar skeletal dysplasia. *J Hum Genet* **76:** 663–671.

Jakobsen LP, Ullmann R, Christensen SB, Jensen KE, Molsted K, Henriksen KF, Hansen C, Knudsen MA, Larsen LA, Tommerup N, et al. 2007. Pierre Robin sequence may be caused by dysregulation of SOX9 and KCNJ2. *J Med Genet* **44:** 381–386.

Jamshidi N, Macciocca I, Dargaville PA, Thomas P, Kilpatrick N, McKinlay Gardner RJ, Farlie PG. 2004. Isolated Robin sequence associated with a balanced t(2;17) chromosomal translocation. *J Med Genet* **41:** e1–e5.

Jin SC, Homsy J, Zaidi S, Lu Q, Morton S, DePalma SR, Zeng X, Qi H, Chang W, Sierant MC, et al. 2017. Contribution of rare inherited and de novo variants in 2,871 congenital heart disease probands. *Nat Genet* **49:** 1593–1601.

Kircher M, Witten DM, Jain P, O'Roak BJ, Cooper GM, Shendure J. 2014. A general framework for estimating the relative pathogenicity of human genetic variants. *Nat Genet* **46:** 310–315.

Lee YH, Saint-Jeannet JP. 2011. Sox9 function in craniofacial development and disease. *Genesis* **49:** 200–208.

Leipoldt M, Erdel M, Bien-Willner GA, Smyk M, Theurl M, Yatsenko SA, Lupski JR, Lane AH, Shanske AL, Stankiewicz P, et al. 2007. Two novel translocation breakpoints upstream of SOX9 define borders of the proximal and distal breakpoint cluster region in campomelic dysplasia. *Clin Genet* **71:** 67–75.

Lek M, Karczewski KJ, Minikel EV, Samocha KE, Banks E, Fennell T, O'Donnell-Luria AH, Ware JS, Hill AJ, Cummings BB, et al. 2016. Analysis of protein-coding genetic variation in 60,706 humans. *Nature* **536:** 285–291.

Mansour S, Offiah A, McDowall S, Sim P, Tolmie J, Hall C. 2002. The phenotype of survivors of campomelic dysplasia. *J Med Genet* **39:** 597–602.

Maroteaux P, Spranger JW, Opitz JM, Kucera J, Lowry RB, Schimke RN. 1971. Le syndrome campomelique. *Presse Med* **22:** 1157–1162.

Matsumoto A, Imagawa E, Miyake N, Ikeda T, Kobayashi M, Goto M, Matsumoto N, Yamagata T, Osaka H. 2017. The presence of diminished white matter and corpus callosal thinning in a case with a SOX9 mutation. *Brain Dev* **40:** 325–329.

McKenna A, Hanna M, Banks E, Sivachenko A, Cibulskis K, Kernytsky A, Garimella K, Altshuler D, Gabriel S, Daly M, et al. 2010. The Genome Analysis Toolkit: a MapReduce framework for analyzing next-generation DNA sequencing data. *Genome Res* **20:** 1297–1303.

Ninomiya S, Isomura M, Narahara K, Seino Y, Nakamura Y. 1996. Isolation of a testes-specific cDNA on Chromosome 17q from a region adjacent to the breakpoint of t(12;17) observed in a patient with campomelic dysplasia and sex reversal. *Hum Mol Genet* **5:** 69–72.

Peng H, Ivanov AV, Oh HJ, Lau YF, Rauscher FJ III. 2009. Epigenetic gene silencing by the SRY protein is mediated by a KRAB-O protein that recruits the KAP1 co-repressor machinery. *J Biol Chem* **284:** 35670–35680.

Pfeifer D, Kist R, Dewar K, Devon K, Lander ES, Birren B, Korniszewski L, Back E, Scherer G. 1999. Campomelic dysplasia translocation breakpoints are scattered over 1 Mb proximal to SOX9: evidence for an extended control region. *Am J Hum Genet* **65:** 111–124.

Savarirayan R, Bankier A. 1998. Acampomelic campomelic dysplasia with de novo 5q;17q reciprocal translocation and severe phenotype. *J Med Genet* **35:** 597–599.

Scott CE, Wynn SL, Sesay A, Cruz C, Cheung M, Gomez Gaviro MV, Booth S, Gao B, Cheah KS, Lovell-Badge R, et al. 2010. SOX9 induces and maintains neural stem cells. *Nat Neurosci* **13:** 1181–1189.

Symon A, Harley V. 2017. SOX9: a genomic view of tissue specific expression and action. *Int J Biochem Cell Biol* **87:** 18–22.

Tommerup N, Schempp W, Meinecke P, Pedersen S, Bolund L, Brandt C, Goodpasture C, Guldberg P, Held KR, Reinwein H, et al. 1993. Assignment of an autosomal sex reversal locus (SRA1) and campomelic dysplasia (CMPD1) to 17q24.3-q25.1. *Nat Genet* **4:** 170–174.

Unger S, Scherer G, Superti-Furga A (2008 [updated: 2013]). Campomelic dysplasia. In *GeneReviews*, pp. 1–17. GeneReviews, University of Washington, Seattle.

Van der Auwera GA, Carneiro MO, Hartl C, Poplin R, Del Angel G, Levy-Moonshine A, Jordan T, Shakir K, Roazen D, Thibault J, et al. 2013. From FastQ data to high confidence variant calls: the Genome Analysis Toolkit best practices pipeline. *Curr Protoc Bioinformatics* **43:** 11 10 11–11 10 33.

Velagaleti GV, Bien-Willner GA, Northup JK, Lockhart LH, Hawkins JC, Jalal SM, Withers M, Lupski JR, Stankiewicz P. 2005. Position effects due to chromosome breakpoints that map approximately 900 Kb upstream and approximately 1.3 Mb downstream of SOX9 in two patients with campomelic dysplasia. *Am J Hum Genet* **76:** 652–662.

Wagner T, Wirth J, Meyer J, Zabel B, Held M, Zimmer J, Pasantes J, Bricarelli FD, Keutel J, Hustert E, et al. 1994. Autosomal sex reversal and campomelic dysplasia are caused by mutations in and around the SRY-related gene SOX9. *Cell* **79:** 1111–1120.

Walters-Sen LC, Thrush DL, Hickey SE, Hashimoto S, Reshmi S, Gastier-Foster JM, Pyatt RE, Astbury C. 2014. Atypical breakpoint in a t(6;17) translocation case of acampomelic campomelic dysplasia. *Eur J Med Genet* **57:** 315–318.

Wang K, Li M, Hakonarson H. 2010. ANNOVAR: functional annotation of genetic variants from high-throughput sequencing data. *Nucleic Acids Res* **38:** e164.

Wang X, Zhou Y, Wang J, Tseng IC, Huang T, Zhao Y, Zheng Q, Gao Y, Luo H, Zhang X, et al. 2016. SNX27 deletion causes hydrocephalus by impairing ependymal cell differentiation and ciliogenesis. *J Neurosci* **36:** 12586–12597.

Wirth J, Wagner T, Meyer J, Pfeiffer RA, Tietze HU, Schempp W, Scherer G. 1996. Translocation breakpoints in three patients with campomelic dysplasia and autosomal sex reversal map more than 130 kb from SOX9. *Hum Genet* **97:** 186–193.

Wunderle VM, Critcher R, Hastie N, Goodfellow PN, Schendl A. 1998. Deletion of long-range regulatory elements upstream of SOX9 causes campomelic dysplasia. *Proc Natl Acad Sci* **95:** 10649–10654.

Yahiro K, Higashihori N, Moriyama K. 2017. Histone methyltransferase Setdb1 is indispensable for Meckel's cartilage development. *Biochem Biophys Res Commun* **482:** 883–888.

Young ID, Zuccollo JM, Maltby EL, Broderick NJ. 1992. Campomelic dysplasia associated with a de novo 2q;17q reciprocal translocation. *J Med Genet* **29:** 251–252.